

# UC San Diego

## UC San Diego Previously Published Works

### Title

Dynamic subcellular translocation of V-type H<sup>+</sup>-ATPase is essential for biomineralization of the diatom silica cell wall

### Permalink

<https://escholarship.org/uc/item/6p7644z7>

### Journal

New Phytologist, 225(6)

### ISSN

0028-646X

### Authors

Yee, Daniel P  
Hildebrand, Mark  
Tresguerres, Martin

### Publication Date

2020-03-01

### DOI

10.1111/nph.16329

Peer reviewed

MR DANIEL YEE (Orcid ID : 0000-0002-2085-5538)

Article type : Regular Manuscript

**Dynamic subcellular translocation of V-type H<sup>+</sup>-ATPase is essential for biomineralization of the diatom silica cell wall**

Daniel P. Yee, Mark Hildebrand\*<sup>†</sup>, Martin Tresguerres<sup>1,\*</sup>

Scripps Institution of Oceanography, University of California San Diego, 9500 Gilman Drive, La Jolla, CA 92093 USA

<sup>1</sup>Corresponding author:

*Martin Tresguerres*

*Tel: (858) 534-5895*

*Email: mtresguerres@ucsd.edu*

\*These authors contributed equally to this work.

Received: *11 September 2019*

Accepted: *4 November 2019*

ORCID

This article has been accepted for publication and undergone full peer review but has not been through the copyediting, typesetting, pagination and proofreading process, which may lead to differences between this version and the [Version of Record](#). Please cite this article as [doi: 10.1111/NPH.16329](https://doi.org/10.1111/NPH.16329)

This article is protected by copyright. All rights reserved

Daniel Yee: <https://orcid.org/0000-0002-2085-5538>

Martin Tresguerres: <https://orcid.org/0000-0002-7090-9266>

†This article is dedicated in memory of Dr Mark Hildebrand (1958–2018), who dedicated his life to advancing the biotechnological applications, and elucidating the beauty and mystery of diatom cell biology.

## Summary

- Diatom cell walls, called frustules, are main sources of biogenic silica in the ocean and their intricate morphology is an inspiration for nanoengineering. Here we show dynamic aspects of frustule biosynthesis involving acidification of the silica deposition vesicle (SDV) by V-type H<sup>+</sup> ATPase (VHA).
- Transgenic *Thalassiosira pseudonana* expressing the VHA B subunit tagged with eGFP (VHA<sub>B</sub>-eGFP) enabled subcellular protein localization in live cells.
- In exponentially growing cultures, VHA<sub>B</sub>-eGFP was present in various subcellular localizations including the cytoplasm, SDVs, and vacuoles. We studied the role of VHA during frustule biosynthesis in synchronized cell cultures of *T. pseudonana*. During the making of new biosilica components, VHA<sub>B</sub>-eGFP first localized in the girdle band SDVs, and subsequently in valve SDVs. In single cell time-lapse imaging experiments, VHA<sub>B</sub>-eGFP localization in SDVs precluded accumulation of the acidotropic silica biomineralization marker PDMPO. Furthermore, pharmacological VHA inhibition prevented PDMPO accumulation in the SDV, frustule biosynthesis, and cell division, as well as insertion of the silicalemma-associated protein SAP1 into the SDVs. Finally, partial inhibition of VHA activity affected the nanoscale morphology of the valve.
- Altogether, these results indicate VHA is essential for frustule biosynthesis by acidifying the SDVs and regulating the insertion of other structural proteins into the SDV.

**Keywords:** biosilica, membrane acidification, protein trafficking, proton pump, silica biomineralization, vacuolar H<sup>+</sup>-ATPase.

## Introduction

Diatoms are a diverse group of eukaryotic phytoplankton found in marine and freshwater ecosystems worldwide, and are responsible for up to 20% of the primary production on the planet (Field *et al.*, 1998). Unique for having a silica cell wall called the frustule, diatoms are the major source of biogenic silica in the ocean and play central roles in oceanic biogeochemical cycling and marine food webs (Barber *et al.*, 1998; Yool & Tyrrell, 2003; Falkowski *et al.*, 2004). The diatom frustule consists of an epitheca and hypotheca that assemble together similar to a Petri dish (Fig. 1)

(Pickett-Heaps *et al.*, 1990). Each half is comprised of a valve on top, and a series of concentric ring-shaped girdle bands on the sides that enable cell elongation. Frustules are synthesized in intracellular compartments called silica deposition vesicles (SDVs), which are defined by a membrane called the silicalemma (Drum & Pankratz, 1964; Volcani & Li, 1984). After cytokinesis a valve is synthesized in each sibling protoplast within an individual SDV close to the cleavage furrow. After valve exocytosis, each girdle band is synthesized in an individual SDV close to the lateral sides of the cell. Silica biomineralization is aided by long-chain polyamines (Poulsen & Kröger, 2004) and proteins located inside SDVs or embedded within the silicalemma, including silicanin-1 (Sin1) (Kotzsch *et al.*, 2017) and silicalemma associated proteins (SAPs) (Tesson *et al.*, 2017), which induce silica polymerization and guide the detailed nanoscale pattern formation of the frustule (Hildebrand *et al.*, 2018); silaffins (Kröger *et al.*, 1999) have also been shown to aid in this process but has not yet been targeted to the SDV.

The SDV is speculated to originate from the Golgi apparatus (Pickett-Heaps *et al.*, 1990) and to expand by the fusing of spherical vesicles to the silicalemma (Schmid & Schulz, 1979). A predicted acidic pH ~5 inside the SDV (Vrieling *et al.*, 1999; Herve *et al.*, 2012) is presumed to slow the polymerization of silicic acid in order to prevent uncontrolled silica deposition and allow for proper morphogenesis of the frustule (Iler, 1979). This level of acidification suggested the involvement of the V-type H<sup>+</sup>-ATPase (VHA) (Gordon & Drum, 1994; Hildebrand *et al.*, 2018), an evolutionary conserved multi-subunit protein complex that uses the energy from ATP hydrolysis to transport H<sup>+</sup> across biological membranes of eukaryotic cells (Nishi & Forgac, 2002; Forgac, 2007). VHA is a holoenzyme that consists of a membrane bound V<sub>0</sub>-domain composed of subunits a, d, e, c, c', c'', and a cytosolic V<sub>1</sub>-domain composed of subunits A-H (Sze *et al.*, 1992, 2002; Kluge *et al.*, 2003; Xiao *et al.*, 2008; Bussard & Lopez, 2014; Tresguerres, 2016). The V<sub>0</sub>-domain forms a proteolipid ring through membranes, and the V<sub>1</sub>-domain hydrolyzes ATP to provide the driving force to move H<sup>+</sup> against its electrochemical gradient (Kawasaki-Nishi *et al.*, 2003).

VHA was first proposed in diatom silicification in the role of acidifying clathrin coated silica transport vesicles to prevent premature hardening of silica prior to delivery to SDV (Gordon & Drum, 1994). Later, a functional study using pharmacological VHA inhibitors would show reduced size and altered morphology in the frustule of the pennate diatom *Phaeodactylum tricorutum* (Vartanian *et*

*al.*, 2009). That study suggested further investigations to confirm whether VHA directly contributed to the regulation of pH in the SDV, study the role of VHA in vesicular trafficking and transport of material to the SDV, and address a potential role of the vacuole in silica biomineralization. However, a following investigation reported the presence of VHA subunit c in the cytoplasm and endoplasmic reticulum (Bussard & Lopez, 2014) rather than the SDV, confounding the potential role of VHA in silicification and suggesting frustule alteration by VHA inhibitors was an indirect effect.

Alternatively, VHA could be present in the silicalemma specifically during frustule formation. Indeed, a change in VHA subcellular localization is a common regulatory mechanism in other organisms; for example, acid/base stress, hormones and neurotransmitters may induce the VHA translocation from the cytoplasm to the cell plasma membrane in kidney (Pastor-Soler *et al.*, 2003), epididymis (Roy *et al.*, 2013), fish gill (Tresguerres *et al.*, 2010; Roa & Tresguerres, 2016), and insect salivary glands (Dames *et al.*, 2006).

To investigate the potential transient location of VHA in the diatom SDV and its role in biomineralization, we generated a transgenic *Thalassiosira pseudonana* cell line expressing VHA subunit B fused to enhanced Green Fluorescent Protein (VHA<sub>B</sub>-eGFP). We then took advantage of a synchronization method (Hildebrand *et al.*, 2007) to determine dynamic changes in VHA subcellular location throughout the cell cycle. In the absence of silicon, *T. pseudonana* cannot make new frustules for the daughter cells and the majority of cells arrests in the Gap 1 (G1) stage of interphase. Four hours after silicon replenishment, ~50% of the cells are in the Gap 2 or mitosis (G2 + M) stages, when cells proceed to perform mitosis, build new valves, and divide (Hildebrand *et al.*, 2007). Five to eight hours after silicon replenishment, the majority of cells in the culture has divided and are in G1 of the next cell division cycle. Frustule biosynthesis was visualized by staining with PDMPO, an acidotropic dye that selectively incorporates into newly biomineralized silica (Shimizu *et al.*, 2001). VHA activity was downregulated by incubating cell cultures with the highly specific pharmacological inhibitor concanamycin A (Dröse & Altendorf, 1997; Huss *et al.*, 2002). Higher temporal resolution of VHA<sub>B</sub>-eGFP translocation to SDVs was visualized by time-lapse super-resolution confocal microscopy. Additionally, we used *T. pseudonana* expressing SAP1-eGFP fusion proteins to interrogate a putative role of VHA activity on the delivery of silicon polymerizing proteins to the SDV. Lastly, wild type *T. pseudonana* cultures were incubated with partial-inhibiting concentrations of concanamycin A and

their frustules imaged using scanning electron microscopy (SEM) to observe effects of VHA activity downregulation on silica biomineralization.

## Materials and Methods

### Culture conditions

*T. pseudonana* (CCMP1335) cultures were grown axenically in ASW medium (Darley & Volcani, 1969) supplemented with 1 mM Na<sub>2</sub>SiO<sub>3</sub>. Wild type and VHA<sub>B</sub>-eGFP expressing cultures were grown on an orbital shaker under continuous illumination by cool-white fluorescent lamps at 70 μmol photons m<sup>-2</sup> s<sup>-1</sup> at 18°C. Cell lines expressing SAP1-eGFP were grown on 16 h : 8 h light : dark cycle to overcome a negative growth phenotype due to light induced overexpression of the SAP1 under control of the *fcp*-promoter.

### Transgenic diatoms expressing fluorescently labeled VHA<sub>B</sub> and SAP1

Proteins labelled with eGFP were expressed under the control of the native or *fcp* promoters. For native expression of Thaps3\_40522 (VHA<sub>B</sub>), DNA fragments including the full-length coding sequence of the gene, 500 bp upstream of the first methionine, and 500 bp downstream of the stop codon were amplified from *T. pseudonana* genomic DNA, and cloned into the Gateway destination vector pMHL\_71 with eGFP at the end of the coding sequence. For *fcp* expression of Thaps3\_40522 (VHA<sub>B</sub>) and Thaps3\_25736 (SAP1), the full-length coding sequence of the gene was amplified from *T. pseudonana* genomic DNA, and cloned into Gateway destination vector pMHL\_79 with eGFP at the end of the coding sequence. All transformation vectors were co-transformed with a pMHL\_09 expressing the *nat1* gene which confers nourseothricin resistance by biolistic gene gun method (Poulsen *et al.*, 2006). Liquid cultures grown in ASW media containing 100 μg/ml nourseothricin were enriched for cells expressing eGFP using several rounds of fluorescence-activated cell sorting on a BD Influx Cell Sorter (BD Biosciences), from which single colonies expressing eGFP were selected for on ASW agar plates containing nourseothricin.

Similar localizations were observed in *T. pseudonana* expressing VHA<sub>B</sub>-eGFP under control of the native (Fig. S1) and *fcp* promoters (Fig. 2), indicating that choice of promoter did not influence localization of the fusion protein. However, cells expressing *fcp*-VHA<sub>B</sub>-eGFP were able to be imaged

longer by fluorescence microscopy and were used for all experiments involving the VHA<sub>B</sub>-eGFP fusion protein.

### **Synchronized cell cycle localization of VHA<sub>B</sub>-eGFP and PDMPO**

For synchronization of the cell cycle, starter cultures of *T. pseudonana* expressing fcp-VHA<sub>B</sub>-eGFP grown to  $2 \times 10^6$  cells ml<sup>-1</sup> were centrifuged at 4,000 g for 10 minutes and washed twice with Si-ASW before being resuspended at  $1.0 \times 10^6$  cells ml<sup>-1</sup> in 500 ml of Si-ASW. Following 24 h of silicon starvation, sodium silicate was added at 200 μM final concentration to initiate cell-cycle progression, and 2-(4-pyridyl)-5-((4-(2-dimethylaminoethyl-aminocarbonyl)methoxy)phenyl)oxazole (PDMPO); LysoSensor YellowBlue DND-160 (Life Technologies) an acidotropic silica biomineralization marker was added at 0.125 μM final concentration to visualize low pH compartments and newly synthesized biosilica. VHA<sub>B</sub>-eGFP and PDMPO localization were tracked in cells sampled from  $t = 0-8$  h at the start of each hour by fluorescence microscopy on a Zeiss Axio Observer.Z1 inverted microscope. Visual analysis and calculations of VHA and PDMPO localization was carried out by recording cells with eGFP signal and/or PDMPO signal in the valve SDV out of the total cell population using the Cell Counts plugin in Fiji (Schindelin *et al.*, 2019). In parallel experiments, 2.5 μl of a 1 mM concanamycin A (AdipoGen BVT-0237; ≥98% purity) stock solution prepared in DMSO was added at 5 nM to 500 ml cell cultures to inhibit VHA activity (Dröse & Altendorf, 1997; Bowman & Bowman, 2002; Huss *et al.*, 2002), equal volumes of DMSO were added in control experiments to account for potential side effects of DMSO on diatom cells. The filter sets used for GFP was Zeiss #38HE (Ex 470/40 nm, FT 495 nm, Em 525/50 nm), PDMPO was Zeiss #21HE (Ex 387/15 nm, FT 409 nm, Em 510/90 nm), and chlorophyll auto-fluorescence was Zeiss #05 (Ex 395-440 nm, FT 460 nm, Em 470 nm).

### **Super-resolution confocal microscopy**

For single cell time-lapse imaging, 2 mL of exponentially growing *T. pseudonana* cell culture expressing VHA<sub>B</sub>-eGFP was transferred to a 35 mm poly-d-lysine coated glass bottom petri dish. Cells were allowed to adhere to the petri dish bottom for 15 mins followed by the addition of 2 mL of ASW medium and PDMPO added for a final concentration of 0.125 μM. Dishes were mounted on a Warner Instruments QE-1HC Quick Exchange Heated/Cooled stage chamber controlled by CL-200



Dual Channel Temperature Controller maintained at 18 °C. Cells were imaged with a Zeiss LSM800 inverted confocal microscope equipped with a Zeiss Plan-Apochromat 63× (1.4) Oil DIC M27 objective, and Zeiss Airyscan super-resolution detector. Two channels were acquired to monitor eGFP (Ex 488 nm with 0.5% laser power, Em 509 nm, detection 490-535 nm) and PDMPO (Ex 335 nm at 0.6% laser power, Em 530 nm, detection 490-575 nm) fluorescence. Images were collected at 3 minute intervals for 4 hours with Zeiss Definite Focus stabilization enabled.

### **VHA<sub>B</sub> mRNA expression**

Thaps3\_40522 (VHA<sub>B</sub>) mRNA expression levels Fragments Per Kilobase Million (FPKM) was acquired from transcriptomics analysis of RNAseq data collected from time-course experiments following silicon replenishment from biological duplicates of synchronized *T. pseudonana* cultures (Abbriano Burke, 2017). Raw reads from individual samples were demultiplexed based on a perfect barcode match, and TopHat (v2.0.6) running Bowtie 2 (version 2.0.2) was used for strand-specific mapping of RNAseq reads to the *T. pseudonana* reference genome assembly (Thaps3) obtained from the Joint Genome Institute (JGI): (<http://genome.jgi.doe.gov/Thaps3/Thaps3.download.ftp.html>). Cufflinks (v.2.2.1) was used to assemble transcripts, and the assembly was used for AUGUSTUS gene model prediction. Raw counts to AUGUSTUS generated gene models were generated using htseq-count (HTSeq 0.6.1p1). Normalized counted and differential expression analysis was done using the DESeq2\_1.6.3 package.

### **VHA<sub>B</sub> protein abundance**

Subsamples of synchronized wildtype *T. pseudonana* expressing VHA<sub>B</sub>-eGFP were harvested at t = 0 before silicon replenishment, and every hour after (t = 1-8 h), by centrifugation on maximum speed at 4°C for 5 minutes followed by freezing of the pellet on dry ice. Protein was extracted in a 2x Extraction Buffer (125 mM Tris pH 6.8 and 138 mM SDS) by boiling at 95°C for 5 minutes, pelleting at max speed, and recovering the supernatant for Western blot analysis. Protein concentration was determined with the BioRad D/C Protein Assay Kit and BSA protein standard. Western Blots were performed by separating 23 µg of total protein in a 10% polyacrylamide mini gel (60 V 20 min, 120 V 90 min) and transferred to a polyvinylidene difluoride (PVDF) membrane. Equivalent protein loading was confirmed by Ponceau staining of total protein on the PVDF membranes (Romero-Calvo *et al.*,

2010). Membranes were blocked in 3% milk blocking buffer and incubated with custom monoclonal VHA<sub>B</sub> primary antibody (1:100) at 4°C overnight. Membranes were washed 3x with T-BST and incubated with goat-anti-mouse HRP antibody (1:10,000) at room temperature for 1 h. Membranes were developed with BioRad Western Clarity ECL and analyzed in a BioRad Universal III Hood using ImageQuant software (BioRad).

### **SEM imaging of frustules**

Wildtype *T. pseudonana* synchronized by silicon starvation was incubated with 200 μM Na<sub>2</sub>SiO<sub>3</sub> for 2 hours, then exposed to 0 (control), 0.4, 1.0, and 2.0 nM concanamycin A for 22 hours. At t = 24 h, 20 ml of each cell culture was pelleted and frozen on dry ice. Frustules were acid washed by resuspending pellets in 50 μl of milli-Q H<sub>2</sub>O (resistivity of 18.2 MΩ.cm at 25°C) and vortexing with 200 μl 100% H<sub>2</sub>SO<sub>4</sub>. Samples were then boiled for 10 minutes, cooled on ice before adding a small amount of KNO<sub>3</sub>, and boiled again for 10 minutes. Next, 800 μl of H<sub>2</sub>O was added to samples before centrifuging at 1,500 g for 10 minutes; the supernatant was discarded. These steps were repeated, without vortexing, to remove all intracellular contents. After washing with H<sub>2</sub>O three times, frustules were resuspended in 200 ml of 100% ethanol for storage and air dried onto stubs at ambient conditions for SEM imaging. Acid cleaned frustules were imaged on Zeiss Sigma 500 SEM at the California Institute for Telecommunications and Information Technology Nano3 facility at UCSD. Quantification of normal and altered valves was completed using the Cell Counts plugin in Fiji (Schindelin *et al.*, 2019).

## **Results**

### **Subcellular localization of VHA<sub>B</sub>-eGFP in *T. pseudonana***

Diatoms expressing VHA<sub>B</sub>-eGFP under control of the *fcp* promoter from exponentially growing (i.e. not synchronized) cultures displayed heterogeneous VHA<sub>B</sub>-eGFP sub-cellular localization. VHA<sub>B</sub>-eGFP was generally found faintly throughout the cytoplasm in all cells. In addition, more concentrated VHA<sub>B</sub>-eGFP signal was present in the silicalemma of girdle band SDVs (Fig. **2a**) and valve SDVs of dividing cells (based on co-localization with PDMPO; Fig. **2b**), or in vacuole tonoplasts (based on co-localization with the vacuolar marker CMAC Ala-Pro; Fig. **2c**).

## VHA<sub>B</sub> mRNA and protein expression in synchronized cell cultures

Next, we quantified VHA<sub>B</sub> mRNA and protein abundance along the cell cycle of *T. pseudonana* cultures synchronized by silicon starvation and replenishment (Fig. 3). Expression of mRNA was measured using an Illumina HiSeq 2000 sequencer. VHA<sub>B</sub> mRNA had a peak at  $t = 4$  h that was ~3.2-fold higher compared to  $t = 0$  h (4,501 vs. 1,391 FPKMs). VHA<sub>B</sub> mRNA abundance then decreased to basal levels (~1116 FPKMs) by  $t = 8$  h. Expression of VHA<sub>B</sub> protein was quantified by Western blotting and revealed two bands, one at ~55 kDa (corresponding to native VHA<sub>B</sub>), and another at ~88 kDa (corresponding to transgenic VHA<sub>B</sub> plus the 33 kDa eGFP tag) (Fig. S2). Native VHA<sub>B</sub> protein abundance had a ~3.2-fold peak between  $t = 3$ -5 hours (Fig. 3). The Western blots also showed that the level of VHA<sub>B</sub>-eGFP protein overexpression over native VHA<sub>B</sub> was moderate, with a maximum of ~2.4 -fold at  $t = 1$  h and nearly equal levels from  $t = 4$  h and onwards.

These mRNA and protein abundance peaks occurred between  $t = 4$ -5 hours which coincided with initiation of valve formation and maximum cell length during the G2 + M phase of the cell cycle observed in previous synchrony experiments conducted with *T. pseudonana* (Hildebrand *et al.*, 2007). While this pattern of VHA<sub>B</sub> expression is consistent with synthesis of new VHA<sub>B</sub> protein for valve SDVs, the presence of VHA<sub>B</sub> in multiple subcellular localization shown in Figure 2 prevents assessing its significance to cell physiology.

## VHA<sub>B</sub>-eGFP and PDMPO localization in SDVs of synchronized cells

To investigate the physiological role of VHA throughout the cell cycle of *T. pseudonana*, VHA<sub>B</sub>-eGFP sub-cellular localization was tracked alongside frustule morphogenesis using the acidotropic silica biomineralization marker PDMPO using fluorescence microscopy. In synchronized cultures, analysis of PDMPO accumulation in the valve SDV in control and concanamycin A-treated cells (Fig. 4a) revealed a strong relationship between VHA<sub>B</sub>-eGFP translocation to the valve SDV, valve formation, and progression of the cell cycle. From  $t = 0$ -3 h after silicon replenishment, VHA<sub>B</sub>-eGFP and PDMPO signal in the valve SDV was minimal, with both occurring in ~5% of the population. The observed peak of roughly one third of the cell population exhibiting both VHA<sub>B</sub>-eGFP and PDMPO in the valve SDV at  $t = 4$  h matches previous reports that the majority of synchronized *T. pseudonana* begin synthesizing the valves 3.5 h after silicon replenishment

(Hildebrand *et al.*, 2007). At  $t = 5$  h, PDMPO signal in newly synthesized valves increased to  $\sim 67\%$  and reached a maximum of  $\sim 88\%$  after  $t = 7$  h. However, VHA<sub>B</sub>-eGFP signal in the valve SDV decreased to  $\sim 14\%$  of the cells at  $t = 5$  h, and then to a minimum of  $\sim 2\%$  by  $t = 8$  h. This is consistent with VHA leaving the silicalemma after the completion of valve synthesis.

### **Dynamics of VHA<sub>B</sub>-eGFP localization and silica biomineralization in SDVs of synchronized cells**

Figure 4b shows representative VHA<sub>B</sub>-eGFP expressing cells corresponding to the hours following silicon replenishment and phases of the cell cycle. In the G1 phase ( $t = 0-2$  h) following silicon replenishment, VHA<sub>B</sub>-eGFP was present throughout the cytoplasm and more prominently in vacuole tonoplasts (Fig. 4bi). Further along in the G1 phase, VHA<sub>B</sub>-eGFP was present in a single girdle band SDV which co-localized with PDMPO marking newly synthesized girdle bands (Fig. 4bii). At the beginning of the G2 + M phase ( $t = 3-6$  h), VHA<sub>B</sub>-eGFP accumulated along with a diffuse signal from PDMPO in the middle of the cell where valve synthesis occurs (Fig. 4biii). Further into the G2 + M phase, VHA<sub>B</sub>-eGFP was present in the valve SDVs while PDMPO signal became concentrated and bound within the newly synthesized valves (Fig. 4biv). VHA<sub>B</sub>-eGFP was maintained in valve SDVs as valve synthesis neared completion (Fig. 4bv). By the end the G2 + M phase, the new PDMPO-labeled valves were exocytosed and the two cells divide. As the daughter cells transitioned to the next G1 phase ( $t = 6-8$  h), VHA<sub>B</sub>-eGFP was again present in girdle band SDVs while a majority of VHA<sub>B</sub>-eGFP was present in tonoplasts, presumably to serve in physiological functions carried out by vacuoles (Fig. 4bvi).

Having established a clear relationship between VHA and SDVs, the functional effect of abolishing VHA activity using the highly specific inhibitor concanamycin A (5 nM) was investigated. Cell cultures treated with concanamycin A displayed no VHA<sub>B</sub>-eGFP signal in SDVs throughout the synchronized time-course (Fig. 4a). Concanamycin A also prevented the accumulation of PDMPO in valves throughout the time-course (Fig. 4a) which indicated that frustule biosynthesis was inhibited, and was consistent with the lack of cell division even after 24 h of exposure to the drug. Cells exposed to concanamycin A showed VHA<sub>B</sub>-eGFP distributed as a diffuse signal throughout the cytoplasm with a slightly denser signal in the middle of the cell, but lacking the concentrated signal typical of

intracellular membrane labelling (Fig. 5a-c). Additional images of concanamycin A treated cells are shown in Supporting Information Fig. S3.

### Live cell time-lapse imaging of VHA<sub>B</sub>-eGFP dynamics

The dynamics of VHA<sub>B</sub>-eGFP translocation in SDVs was investigated using time-lapse super-resolution confocal fluorescence microscopy analysis of single *T. pseudonana* cells expressing fcp-VHA<sub>B</sub>-eGFP incubated with PDMPO during the G2 + M phase (corresponding to t = 4 h of the synchrony, and defined here as t = 0 min) (Fig. 6). At t = 0 min, VHA<sub>B</sub>-eGFP was predominantly in the tonoplasts of two adjacent vacuoles. At t = 6 min, a distinct VHA<sub>B</sub>-eGFP signal began to accumulate at the center of the cell marking the membranes of two adjacent valve SDVs. Three minutes later at t = 9 min, PDMPO began to mark new valves and VHA<sub>B</sub>-eGFP signal expanded further along the middle region of the cell. By t = 27 min, VHA<sub>B</sub>-eGFP had made its way across the entire middle plane and a strong co-localization with PDMPO became visible. By t = 66 min the VHA signal in the SDVs began to decrease while PDMPO remained trapped within mature valve biosilica. At t = 93 min, VHA<sub>B</sub>-eGFP signal in the SDV was nearly absent, and by t = 111 min, VHA<sub>B</sub>-eGFP was only faintly visible in the plasma membrane of each daughter cell. VHA<sub>B</sub>-eGFP signal was always present in vacuole tonoplasts which appeared to be associated with the valve SDVs up until t = 93 min. A movie of this time-lapse can be found in Supporting Information Video S1.

The VHA<sub>B</sub>-eGFP dynamics in girdle band SDVs was captured in two attached daughter cells in the G1 phase (Fig. 7), this approach was adopted to consistently identify cells in the G1 phase following valve biosynthesis in the G2 + M phase for high magnification focusing for super-resolution imaging. At t = 0 min, each cell already had newly synthesized girdle bands which extend from the valves and are labeled with PDMPO. In the top cell, VHA<sub>B</sub>-eGFP was concentrated in the vacuole tonoplasts which could be seen in close association with a new girdle band SDV (similar to the association with the valve SDVs show in Figure 6). From t = 24-57 min, VHA<sub>B</sub>-eGFP co-localized with PDMPO in girdle band SDVs. By t = 60 min, VHA<sub>B</sub>-eGFP had left the girdle band SDV while PDMPO remained in the newly synthesized girdle band. Similar observations were made in the lower cell, but was delayed by ~10 minutes relative to the top cell. A movie of this time-lapse

showing the completion of both upper and lower girdle bands can be found in Supporting Information Video S2.

### **Effects of VHA inhibition on SAP1 incorporation into the SDV**

Next, we examined whether VHA activity is required for the incorporation of the structural protein SAP1 into SDVs in cultures of *T. pseudonana* expressing fcp-SAP1-eGFP. First, we confirmed the previously described localization of SAP1 (Tesson *et al.*, 2017) in the silicalemmas of SDVs of both girdle bands (Fig. 8a) and valves (Fig. 8b). In dividing cells, SAP1 appeared to be trafficked through the cytoplasm in a single vesicle that attached to valve SDVs and fused into the silicalemma (Fig. S4a-f). Following cytokinesis, SAP1 was again found within a single vesicle adjacent to newly formed valves in each daughter cell (Fig. 8c). However, in cells exposed to 5 nM concanamycin A, SAP1 accumulated in the middle of the cell, in multiple vesicles that varied in size (Fig. 8d-f; Fig. S4g-l). Similar to the VHA inhibition experiments captured in Figures 4a and 5, 5 nM concanamycin A prevented PDMPO accumulation in SDVs, indicating inhibition of frustule biosynthesis. However, intense PDMPO signal was observed in a few SAP1-containing vesicles (Fig. 8f), suggesting they were acidic and that silica may have biomineralized in those compartments despite VHA inhibition. We tentatively suggest this is related to SAP1 overexpression.

### **Effects of VHA inhibition on valve nanostructure**

Finally, we exposed *T. pseudonana* cultures to submaximal concanamycin A concentrations (0-2 nM) to examine the effects of reduced VHA activity on growth and valve ultrastructure. A dose-response growth curve revealed that cultures exposed to 0.4 nM concanamycin A resulted in a ~25% decrease in growth rate and ~36% decrease in final cell density compared to the control treatment (Fig. 9a). About one quarter of the valves from diatoms exposed to 0.4 nM concanamycin displayed altered morphology, while the remaining valves were likely synthesized before exposure to concanamycin A and therefore looked normal. Compared to valves from control diatoms (Fig. 9b), altered valves exhibited decreased deposition of silica, and lacked features characteristic of the distal surface of valves (Fig. 9c-e). While ribs were present in the altered valves, they lacked defined ridges and were composed of more granular silica nanoparticles. As a result of reduced silica deposition, some of the valves were bent at the edges making them less round (Fig. 9c), suggesting a decrease in

rigidity. The portula was also deformed and the fulcra were mis-located away from the outer edges, and found closer to the center of the valve (Fig. 9c). Sub-optimal VHA activity additionally affected the nanopore-containing space in between ribs (Fig. 9e): in some frustules it was only partially filled, and in the most extreme cases it was entirely absent. Additional images of altered valves are shown in Supporting Information Fig. S5.

## Discussion

Our results demonstrate that VHA is responsible for the acidification of *T. pseudonana* SDVs which is essential for silica biomineralization *in vivo*, and identify the dynamic translocation of VHA to SDVs as a novel mechanism for frustule biosynthesis. Combining transgenic diatoms expressing VHA<sub>B</sub>-eGFP and synchronization of cell cycle by silicon depletion and replenishment allowed us to study the order of events that lead to SDV acidification, silicon biomineralization, and cell division. Under our experimental conditions, the average duration of the cell cycle is ~8h. During G1 (t = 0-2 h after silicon replenishment), VHA<sub>B</sub>-eGFP is found in the cytoplasm and concentrated in vacuole tonoplasts then to girdle band SDVs for the synthesis of girdle bands which expand the cell. At the onset of G2 and during mitosis (t = 3-6 h), VHA<sub>B</sub>-eGFP translocates from vacuoles to valve SDVs of each daughter cell to produce the two new valves required for the cells to separate. Time-lapse imaging using super-resolution confocal microscopy showed that VHA<sub>B</sub>-eGFP presence in the SDV precedes accumulation of the acidotropic dye PDMPO, which in turn is completely abolished by the highly specific VHA inhibitor concanamycin A. Altogether, this indicates that VHA acidifies the SDV and that this acidification is essential for frustule biosynthesis. After the new valves are exocytosed (t = 6-8 h), cells enter G1 of the next cell cycle and VHA<sub>B</sub>-eGFP is turned over by translocating to the plasma membrane, leaving behind PDMPO-labeled frustules and confirming the dynamic nature of VHA. These results support the previous suggestion that the SDV integrates with the plasma membrane after frustule exocytosis (Kotzsch *et al.*, 2017).

The essential role of VHA activity on diatom frustule formation is due to at least two potential processes. First, VHA likely provides the acidic pH that has long been predicted inside the SDV which may aid in shaping and arranging silica nanospheres, and enabling the proper function of silica forming proteins (Iler, 1979; Kröger *et al.*, 1999; Kröger *et al.*, 2000, 2002; Sumper & Kröger, 2004;

Kotzsch *et al.*, 2017). While P-type H<sup>+</sup>-ATPases have been identified in diatoms (Bussard & Lopez, 2014), they are not inhibited at the nanomolar concentrations of concanamycin A used in our study (Dröse & Altendorf, 1997). Given the specificity of concanamycin A for VHA, and its suppressive effect on frustule synthesis as well as cell division in cultures, our results suggest that VHA is the only proton pump involved in SDV acidification. Second, VHA inhibition blocked the delivery of SAP1-containing vesicles to SDVs, pointing out a potential role of VHA in regulating vesicle fusion to the silicalemma. This function may depend on SDV acidification itself or on the recruitment of the vesicle fusion machinery by VHA as reported in other cells (Maxson & Grinstein, 2014). If this is true, another outstanding question is whether VHA activity is required for the fusion of vesicles trafficking other components to the SDV of newly forming frustules including other structural proteins found in SDV membranes and substrates of the insoluble organic matrices known to comprise frustules (Tesson & Hildebrand, 2013; Kotzsch *et al.*, 2016). Alternatively, inhibition of VHA by concanamycin A may prevent SDV formation, leaving SDV associated proteins without a final location to target to.

In addition to the SDV, we found that VHA<sub>B</sub>-eGFP is present in the vacuole tonoplast in cells in various cell stages (Figs. **2c**, **4b**, **6-7**), which opens new questions about the regulatory mechanisms behind differential VHA subcellular localization and coordination of vacuolar function and cell division. Interestingly, the tonoplast appeared to maintain an association with the SDV, and may act as a reservoir for newly synthesized VHA. The proximity of vacuoles near locations of valve and girdle band synthesis suggests the transfer of VHA-containing tonoplast to the silicalemma during valve biogenesis, providing insights into the potential origin of SDV membrane material such as lipids and other proteins. In cultures treated with a fully inhibiting dose of concanamycin A, cells that were in the process of dividing had increased VHA<sub>B</sub>-eGFP in the site where the new valves would form; however, they lacked a defined SDV (Fig. **5a-c**; Fig. **S3**). In these cells, we hypothesize that VHA<sub>B</sub>-eGFP was localized in a non-rigid SDV membrane representative of an early stage in valve formation, which is consistent with previous observations of very early stages of valve formation with deformed but recognizable silica structure (Hildebrand, 2010) and a folded appearance similar to a “taco” shell (Hildebrand *et al.*, 2007). An interesting concept to consider is whether the normal SDV shape directly depends on VHA activity. To prevent aberrant valve structure, the SDV must become fully expanded prior to or at least concurrent with completion of the base layer. Thus, SDV expansion would be a



property of the organic material comprising the SDV, and not the silica itself. In addition, several *T. pseudonana* silicification proteins exhibit reversible aggregation as pH is decreased (Kotzsch *et al.*, 2016, 2017), suggesting VHA-dependent acidification induces protein aggregation and organization inside the SDV, resulting in a subsequent change in SDV topology and expansion.

The halting of cell division by a high concanamycin A dose together with the presence of VHA<sub>B</sub>-eGFP in multiple subcellular compartments unfortunately prevented the generation of VHA gene knockouts due to lack of growth and potential unspecific effects on other physiological processes, respectively. As an alternative, we examined the effect of VHA pharmacological knockdown on valve morphology by growing synchronized *T. pseudonana* cultures in a partially inhibiting concanamycin A dose. These cells divided at about 75% the normal rate which yielded a mix of normal valves that were generated before the addition of concanamycin A, and newly formed valves with an abnormal morphology. While the ribs in the silica base layer had relatively minor malformations, the nanopore network in the areas between the ribs was partially or entirely missing, and the portula and fuloportulae were deformed and occasionally displaced from their normal locations. These results suggest that a fully acidified SDV is more essential for maturation of the distal surface ridges above the ribs of the valves and porous base layer of nanopores. Interestingly, a SAP1 knockdown (Tesson *et al.*, 2017) and Sin1 knockout (Görlich *et al.*, 2019) also resulted in aberrant patterning deposition of the silica network in the distal valve surface, further supporting the link between VHA function and recruitment of SAP1-containing vesicles to the SDV.

## Conclusion

This study confirms the decades-long hypotheses (Gordon & Drum, 1994) that VHA is the enzyme directly responsible for SDV acidification *in vivo*. It also identified that VHA activity regulates the trafficking and fusion of vesicles containing the structural protein SAP1 into the SDV, and revealed that frustule formation is a highly dynamic process that includes intimate interactions between SDVs and vacuoles. In addition to revealing those novel basic mechanistic aspects of diatom frustule biosynthesis, this study has identified interesting areas for future research: is VHA activity important for the trafficking of other proteins to the SDV or biogenesis of the SDV? What is the function of VHA in the vacuole? What are the regulatory mechanisms behind differential VHA

subcellular localization throughout the cell cycle? Can we take advantage of this information to manipulate VHA activity and nanoengineer frustules with specific porosity, silica nanosphere size, and ornamentation?

The dominance of diatoms over other phytoplankton groups is presumed to be due, in part, to their ability to use silica as a substrate for growth. Compared to carbon, making cell walls out of silica provides energy savings (Raven, 1983), and silica cell walls have been proposed to act as a pH buffer to provide more CO<sub>2</sub> and promote photosynthesis (Milligan & Morel, 2002). Thus, understanding the mechanisms responsible for diatom silicification carries broader implications for understanding the role of diatoms in the global carbon cycle and primary production in the oceans.

### **Acknowledgements**

The project described was supported by awards from the National Institute of Health Training Grant in Marine Biotechnology (T32GM067550) and the Edna Bailey Sussman Foundation to DPY, and the UCSD Frontiers of Innovation Scholars Program to MT. We would like to thank Dr. Roshan Shreshta for providing plasmids and assisting with diatom cloning and transformations, Dr. Raffaella Abbriano Burke for analysis of RNAseq data, and Dr. Amro Hamdoun for providing advice on live cell imaging.

### **Author Contributions**

DPY, MH, and MT designed research; DPY performed research; DPY, MH, and MT analyzed data and interpreted results; and DPY, MH, and MT wrote the manuscript. MH and MT contributed equally to this work.

### **References**

- Abbriano Burke R. 2017.** *Insights into the molecular regulation of growth and carbon flux in marine diatoms*. PhD thesis, University of California, San Diego, La Jolla, CA, USA.
- Barber RT, Falkowski PG, Barber RT, Smetacek V. 1998.** Biogeochemical controls and feedbacks on ocean primary production. *Science* **281**: 200–207.

**Bowman BJ, Bowman EJ. 2002.** Mutations in subunit c of the vacuolar ATPase confer resistance to bafilomycin and identify a conserved antibiotic binding site. *Journal of Biological Chemistry* **277**: 3965–3972.

**Bussard A, Lopez PJ. 2014.** Evolution of vacuolar pyrophosphatases and vacuolar H<sup>+</sup>-ATPases in diatoms. *Journal of Marine Science and Technology* **22**: 50–59.

**Dames P, Zimmermann B, Schmidt R, Rein J, Voss M, Schewe B, Walz B, Baumann O. 2006.** cAMP regulates plasma membrane vacuolar-type H<sup>+</sup>-ATPase assembly and activity in blowfly salivary glands. *Proceedings of the National Academy of Sciences* **103**: 3926–3931.

**Darley WM, Volcani BE. 1969.** Role of silicon in diatom metabolism: a silicon requirement for deoxyribonucleic acid synthesis in the diatom *Cylindrotheca fusiformis* Reimann and Lewin. *Experimental Cell and Research* **58**: 334–342.

**Dröse S, Altendorf K. 1997.** Bafilomycins and concanamycins as inhibitors of V-ATPases and P-ATPases. *Journal of Experimental Biology* **8**: 1–8.

**Drum RW, Pankratz HS. 1964.** Post mitotic fine structure of *Gomphonema parvulum*. *Journal of ultrastructure research* **10**: 217–223.

**Falkowski PG, Grzebyk D, Katz ME, Knoll AH, Quigg A, Raven JA, Schofield O, Taylor FJR. 2004.** The evolution of modern eukaryotic phytoplankton. *Science* **305**: 354–360.

**Field CB, Behrenfeld MJ, Randerson JT, Falkowski PG. 1998.** Primary production of the biosphere: Integrating terrestrial and oceanic components. *Science* **281**: 237–240.

**Forgac M. 2007.** Vacuolar ATPases : rotary proton pumps in physiology and pathophysiology. *Nature Reviews Molecular Cell Biology* **8**: 917–929.

**Gordon R, Drum RW. 1994.** The chemical basis of diatom morphogenesis. *International Review of Cytology* **150**: 243–372.

**Görlich S, Pawolski D, Zlotnikov I, Kröger N. 2019.** Control of biosilica morphology and mechanical performance by the conserved diatom gene Silicanin-1. *Communications Biology* **2**: 1–8.

**Herve V, Derr J, Quinet M, Moisan L, Lopez PJ. 2012.** Multiparametric analyses reveal the pH-dependence of silicon biomineralization in diatoms. *PLoS ONE* **7**: e46722.

**Hildebrand M. 2010.** 3D imaging of diatoms with ion-abrasion electron microscopy. *Journal of Structural Biology* **166**: 316–328.

**Hildebrand M, Frigeri LG, Davis AK. 2007.** Synchronized growth of *Thalassiosira Pseudonana* (*Bacillariophyceae*) provides novel insights into cell-wall synthesis processes in relation to the cell cycle. *Journal of Phycology* **740**: 730–740.

**Hildebrand M, Lerch SJL, Shrestha RP. 2018.** Understanding diatom cell wall silicification—moving forward. *Frontiers in Marine Science* **5**: 1–19.

**Huss M, Ingenhorst G, Ko S, Gaßel M, Dro S, Zeeck A, Altendorf K, Wiczorek H. 2002.** Concanamycin A, the specific inhibitor of V-ATPases, binds to the V<sub>o</sub> subunit c. *Journal of Biological Chemistry* **277**: 40544–40548.

**Iler RK. 1979.** *The Chemistry of Silica: Solubility, Polymerization, Colloid and Surface Properties, and Biochemistry*. New York: Wiley-Interscience.

**Kawasaki-Nishi S, Nishi T, Forgac M. 2003.** Proton translocation driven by ATP hydrolysis in V-ATPases. *FEBS Letters* **545**: 76–85.

**Kluge C, Lahr J, Hanitzsch M, Bolte S, Gollack D, Dietz K. 2003.** New insight into the structure and regulation of the plant vacuolar H<sup>+</sup>-ATPase. *Journal of Bioenergetics and Biomembranes* **35**: 377–388.

**Kotzsch A, Gröger P, Pawolski D, Bomans PHH, Sommerdijk NAJM, Schlierf M, Kröger N. 2017.** Silicanin-1 is a conserved diatom membrane protein involved in silica biomineralization. *BMC Biology* **15**: 65.

**Kotzsch A, Pawolski D, Milentyev A, Shevchenko A, Scheffel A, Poulsen N, Shevchenko A, Kröger N. 2016.** Biochemical composition and assembly of biosilica-associated insoluble organic matrices from the diatom *Thalassiosira pseudonana*. *Journal of Biological Chemistry* **291**: 4982–4997.

**Kröger N, Deutzmann R, Bergsdorf C, Sumper M. 2000.** Species-specific polyamines from diatoms control silica morphology. *Proceedings of the National Academy of Sciences* **97**: 14133–14138.

**Kröger N, Deutzmann R, Sumper M. 1999.** Polycationic peptides from diatom biosilica that direct silica nanosphere formation. *Science* **286**: 1129–1132.

**Kröger N, Lorenz S, Brunner E, Sumper M. 2002.** Self-assembly of highly phosphorylated silaffins and their function in biosilica morphogenesis. *Science* **298**: 584–586.

**Maxson ME, Grinstein S. 2014.** The vacuolar-type H<sup>+</sup>-ATPase at a glance - more than a proton pump. *Journal of Cell Science* **127**: 4987–4993.

**Milligan AJ, Morel FMM. 2002.** A proton buffering role for silica in diatoms. *Science* **297**: 1848–1850.

**Nishi T, Forgac M. 2002.** The vacuolar (H<sup>+</sup>)-ATPases — nature's most versatile proton pumps. *Nature Reviews Molecular Cell Biology* **3**: 94–103.

**Pastor-Soler N, Beaulieu V, Litvin TN, Da Silva N, Chen Y, Brown D, Buck J, Levin LR, Breton S. 2003.** Bicarbonate-regulated adenylyl cyclase (sAC) is a sensor that regulates pH-dependent V-ATPase recycling. *The Journal of Biological Chemistry* **278**: 49523–49529.

**Pickett-Heaps JD, Schmid AMM, Edgar LA. 1990.** *The cell biology of diatom valve formation* (FE Round and DJ Chapman, Eds.). Bristol. Biopress Ltd.

**Poulsen N, Chesley PM, Kröger N. 2006.** Molecular genetic manipulation of the diatom *Thalassiosira pseudonana* (Bacillariophyceae). *Journal of Phycology* **42**: 1059–1065.

**Poulsen N, Kröger N. 2004.** Silica morphogenesis by alternative processing of silaffins in the diatom *Thalassiosira pseudonana*. *Journal of Biological Chemistry* **279**: 42993–42999.

**Raven JA. 1983.** The transport and function of silicon in plants. *Biological Reviews* **58**: 179–207.

**Roa JN, Tresguerres M. 2016.** Soluble adenylyl cyclase is an acid-base sensor in epithelial base-secreting cells. *American Journal of Physiology - Cell Physiology* **311**: C340–C349.

**Romero-Calvo I, Ocón B, Martínez-Moya P, Suárez MD, Zarzuelo A, Martínez-Augustin O, de Medina FS. 2010.** Reversible Ponceau staining as a loading control alternative to actin in Western blots. *Analytical Biochemistry* **401**: 318–320.

**Roy JW, Hill E, Ruan YC, Vedovelli L, Paunescu TG, Brown D, Breton S. 2013.** Circulating aldosterone induces the apical accumulation of the proton pumping V-ATPase and increases proton secretion in clear cells in the caput epididymis. *American Journal of Physiology - Cell Physiology* **305**: C436–C446.

**Schindelin J, Arganda-carreras I, Frise E, Kaynig V, Longair M, Pietzsch T, Preibisch S, Rueden C, Saalfeld S, Schmid B, et al. 2019.** Fiji : an open-source platform for biological-image analysis. *Nature Methods* **9**: 676–682.

**Schmid AMM, Schulz D. 1979.** Wall morphogenesis in diatoms: Deposition of silica by cytoplasmic vesicles. *Protoplasma* **100**: 267–288.

**Shimizu K, Del Amo Y, Brzezinski MA, Stucky GD, Morse DE. 2001.** A novel fluorescent silica tracer for biological silicification studies. *Chemistry and Biology* **8**: 1051–1060.

**Sumper M, Kröger N. 2004.** Silica formation in diatoms: the function of long-chain polyamines and silaffins. *Journal of Materials Chemistry* **14**: 2059–2065.

**Sze H, Schumacher K, Müller ML, Padmanaban S, Taiz L. 2002.** A simple nomenclature for a complex proton pump: VHA genes encode the vacuolar H<sup>+</sup>-ATPase. *Trends in Plant Science* **7**: 157–161.

**Sze H, Ward JM, Lai S. 1992.** Vacuolar H<sup>+</sup>-translocating ATPases from plants: Structure, function, and isoforms. *Journal of Bioenergetics and Biomembranes* **24**: 371–381.

**Tesson B, Hildebrand M. 2013.** Characterization and localization of insoluble organic matrices associated with diatom cell walls : Insight into their roles during cell wall formation. *PLoS ONE* **8**: e61675.

**Tesson B, Lerch SJL, Hildebrand M. 2017.** Characterization of a new protein family associated with the silica deposition vesicle membrane enables genetic manipulation of diatom silica. *Scientific*

*Reports* 7: 1–13.

**Tresguerres M. 2016.** Novel and potential physiological roles of vacuolar-type H<sup>+</sup>-ATPase in marine organisms. *The Journal of Experimental Biology* **219**: 2088–2097.

**Tresguerres M, Parks SK, Salazar E, Levin LR, Goss GG, Buck J. 2010.** Bicarbonate-sensing soluble adenylyl cyclase is an essential sensor for acid/base homeostasis. *Proceedings of the National Academy of Sciences* **107**: 442–447.

**Vartanian M, Desclés J, Quinet M, Douady S, Lopez PJ. 2009.** Plasticity and robustness of pattern formation in the model diatom *Phaeodactylum tricornutum*. *New Phytologist* **182**: 429–442.

**Volcani BE, Li CW. 1984.** Aspects of silicification in wall morphogenesis of diatoms. *Philosophical Transactions of the Royal Society B: Biological Sciences* **304**: 519–528.

**Vrieling EG, Gieskes WWC, Beelen TPM. 1999.** Silicon deposition in diatoms: Control by the pH inside the silicon deposition vesicle. *Journal of Phycology* **35**: 548–559.

**Xiao Y-T, Xiang L-X, Shao J-Z. 2008.** Vacuolar H<sup>+</sup>-ATPase. *International Journal of Biochemistry and Cell Biology* **40**: 2002–2006.

**Yool A, Tyrrell T. 2003.** Role of diatoms in regulating the ocean's silicon cycle. *Global Biogeochemical Cycles* **17**: 1–21.

## Figure legends

**Fig. 1** Diagram of a centric diatom undergoing cell division. The frustule is composed of a hypotheca and overlapping epitheca which encapsulates the cell membrane and all other intracellular compartments. Each theca is composed of a valve and concentric rings of girdle bands. During the M phase following cytokinesis, two valves are synthesized within silica deposition vesicles (SDVs) of two daughter cells and separate the cells when exocytosed. Py, the pyrenoid.

**Fig. 2** V-type H<sup>+</sup> ATPase (VHA) localization in multiple subcellular compartments. Representative images of exponentially growing *Thalassiosira pseudonana* expressing fcp-VHA<sub>B</sub>-eGFP in (a) a

girdle band silica deposition vesicle (SDV), **(b)** valve SDVs, and **(c)** vacuole tonoplast. Green, VHA<sub>B</sub>-eGFP; red, chlorophyll; magenta, PDMPO **(a-b)**, CMAC-Ala-Pro **(c)**; white, colocalization of VHA<sub>B</sub>-eGFP and PDMPO **(a-b)**. Scale bar: 5  $\mu$ m.

**Fig. 3** Relative VHA<sub>B</sub> protein abundance (n=5; error bars=  $\pm$ SE) and mRNA expression (FPKM) from synchronized *Thalassiosira pseudonana* cultures following silicon replenishment.

**Fig. 4 (a)** V-type H<sup>+</sup> ATPase (VHA) dynamics in the valve-specific silica deposition vesicles (SDVs) throughout the cell cycle. Percentage of cells with VHA<sub>B</sub>-eGFP in the valve specific SDVs, PDMPO signal in valves in control and concanamycin A treated cultures. VHA and PDMPO localization was analyzed using the Cell Counter tool in ImageJ on  $\sim$ 280 cells per time point ( $\sim$ 2500 cells total; n=3; error bars =  $\pm$ SE). **(b)** Representative cell images of VHA<sub>B</sub> subcellular localization throughout the cell cycle in *Thalassiosira pseudonana* expressing fcp-VHA<sub>B</sub>-eGFP: **(i)** cytoplasmic and tonoplast localization, **(ii)** tonoplast and girdle band SDV localization during G1 phase, **(iii)** accumulation at the site of valve biosynthesis, initial **(iv)** and later stage **(v)** concentration in the valve SDVs during G2 + M phase, **(vi)** cytoplasmic, girdle band SDV, and tonoplast localization in the G1 phase of two daughter cells. Green: VHA<sub>B</sub>-eGFP; magenta: PDMPO; white: colocalization of VHA<sub>B</sub>-eGFP and PDMPO; red: chlorophyll; differential interference contrast. Yellow arrows in **vi** indicate girdle bands. Scale bar: 5  $\mu$ m.

**Fig. 5** Inhibition of V-type H<sup>+</sup> ATPase (VHA) activity prevents frustule biosynthesis. **(a-c)** Representative images of synchronized *Thalassiosira pseudonana* expressing fcp-VHA<sub>B</sub>-eGFP treated with 5 nM concanamycin A. Green, VHA<sub>B</sub>-eGFP; magenta, PDMPO; white, colocalization of VHA<sub>B</sub>-eGFP and PDMPO; red, chlorophyll; DIC, differential interference contrast. Yellow arrowheads highlight VHA accumulation near the location where the valve biosynthesis normally occurs. Scale bar: 5  $\mu$ m.

**Fig. 6** Time-lapse during valve biosynthesis. Selected images from time-lapse super resolution confocal fluorescence microscopy of *Thalassiosira pseudonana* expressing fcp-VHA<sub>B</sub>-eGFP incubated with PDMPO are shown during valve biosynthesis (Supporting information **Video S1**). Green, VHA<sub>B</sub>-eGFP; magenta, PDMPO; white, colocalization of VHA<sub>B</sub>-eGFP and PDMPO. Yellow



arrowheads highlight association of vacuoles with silica deposition vesicles (SDVs). Scale bar: 2.5  $\mu\text{m}$ .

**Fig. 7** Time-lapse during girdle band biosynthesis. Selected images from time-lapse super resolution confocal fluorescence microscopy of two attached *Thalassiosira pseudonana* cells expressing fcp-VHA<sub>B</sub>-eGFP incubated with PDMPO are shown during girdle band biosynthesis (Supporting information **Video S2**). Green, VHA<sub>B</sub>-eGFP; magenta, PDMPO; white, colocalization of VHA<sub>B</sub>-eGFP and PDMPO. Yellow arrowheads highlight association of vacuoles with SDVs. Scale bar: 2.5  $\mu\text{m}$ .

**Fig. 8** Inhibition of V-type H<sup>+</sup> ATPase (VHA) activity prevents insertion of SAP1 into the silica deposition vesicle (SDV). Representative images of cell cycle synchronized *Thalassiosira pseudonana* expressing fcp-SAP1-eGFP. **(a-c)** Control cells. **(d-f)** Cells incubated with 5 nM concanamycin A. Green, SAP1-eGFP; magenta, PDMPO; white, colocalization of SAP1-eGFP and PDMPO; red, chlorophyll; DIC, differential interference contrast. Yellow arrowheads highlight SAP1 near the location where the valve biosynthesis normally occurs. Red arrow highlights the concentration of PDMPO in SAP1 vesicles. Scale bar: 5  $\mu\text{m}$ .

**Fig. 9** Suboptimal V-type H<sup>+</sup> ATPase (VHA) activity results in abnormal valve nanostructure. **(a)** Growth curves of *Thalassiosira pseudonana* cultures under various concanamycin A concentrations (n = 2; error bars = SE). Valve nanostructure was examined by scanning electron microscopy after 22h growth in **(b)** control or **(c-e)** 0.4 nM concanamycin A conditions. **(b-c)** Insets shows central portula at  $\times 2$  magnification, white arrowheads, central portula; **(c)** yellow arrowhead, displaced fuloportula; **(e)** blue arrowhead, ribs lacking ridges; red arrowhead, unfilled nanopore base layer. Scale bars: 1  $\mu\text{m}$  for panels **b-d** and 0.5  $\mu\text{m}$  for panel **e**.

### Supporting Information

**Fig. S1** Representative images of exponentially growing *T. pseudonana* natively expressing VHA<sub>B</sub>-eGFP.

**Fig. S2** Western blots of VHA<sub>B</sub> protein abundance in *T. pseudonana* cultures throughout the cell cycle along with corresponding Ponceau stained blots.

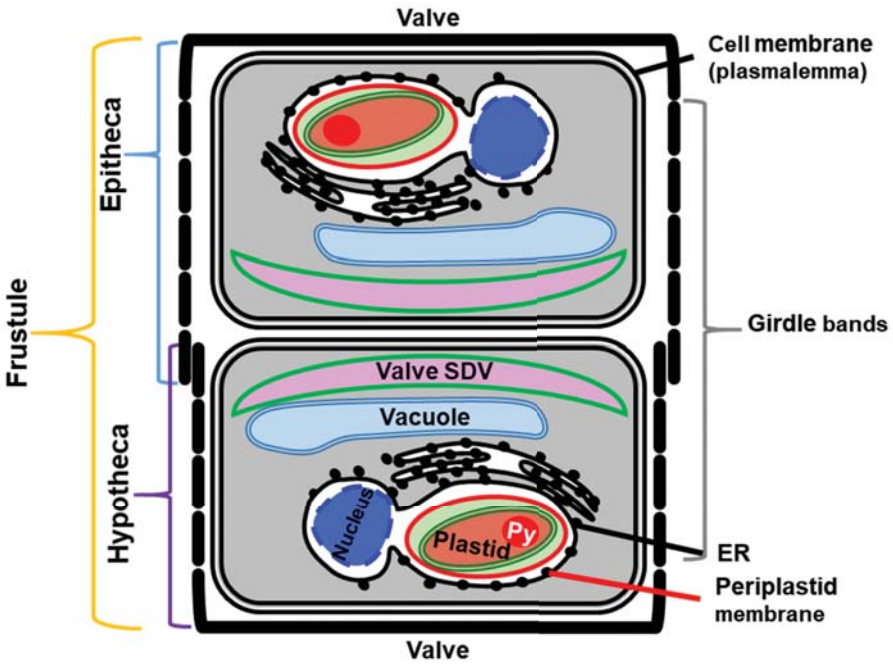
**Fig. S3** Representative images of cell cycle synchronized *T. pseudonana* expressing fcp-VHA<sub>B</sub>-eGFP incubated with 5 nM concanamycin A.

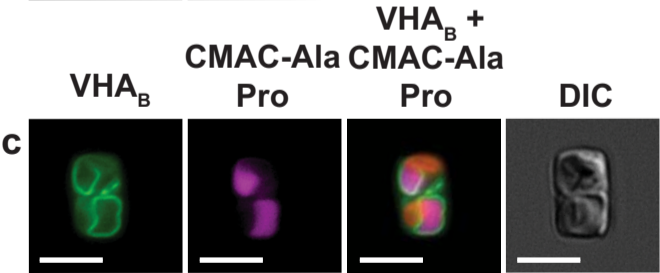
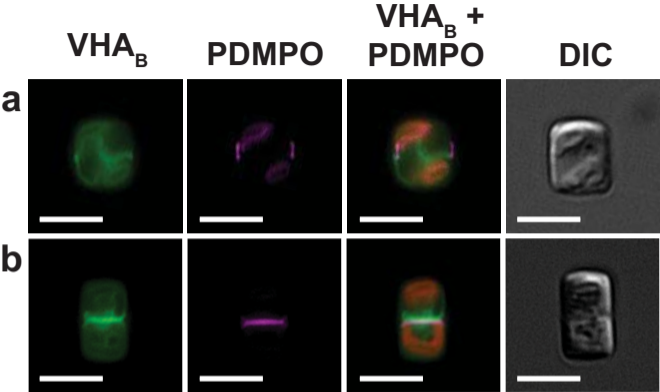
**Fig. S4** Representative images of cell cycle synchronized *T. pseudonana* expressing fcp-SAP1-eGFP -/+ 5 nM concanamycin A.

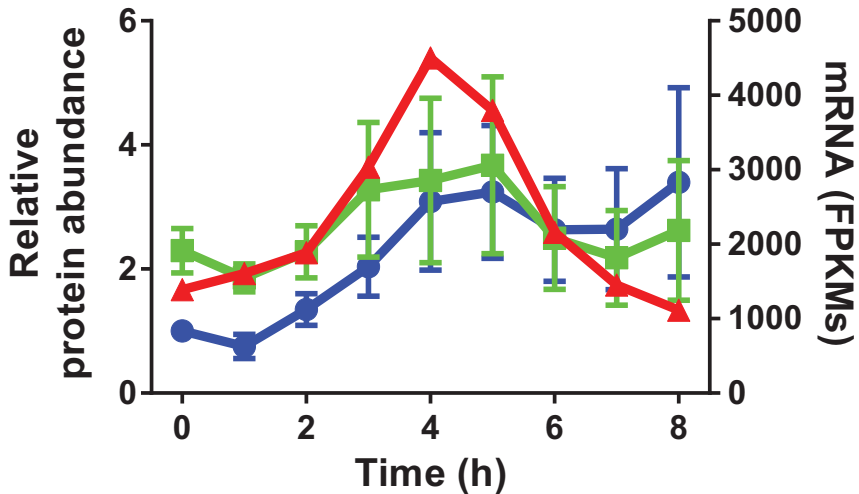
**Fig. S5** Suboptimal VHA activity results in altered valve nanostructure, examined by SEM after 22h growth with 0.4 nM concanamycin A conditions.

**Video S1** Time-lapse imaging video of *T. pseudonana* expressing fcp-VHA<sub>B</sub>-eGFP during valve biosynthesis [MP4 803 kb].

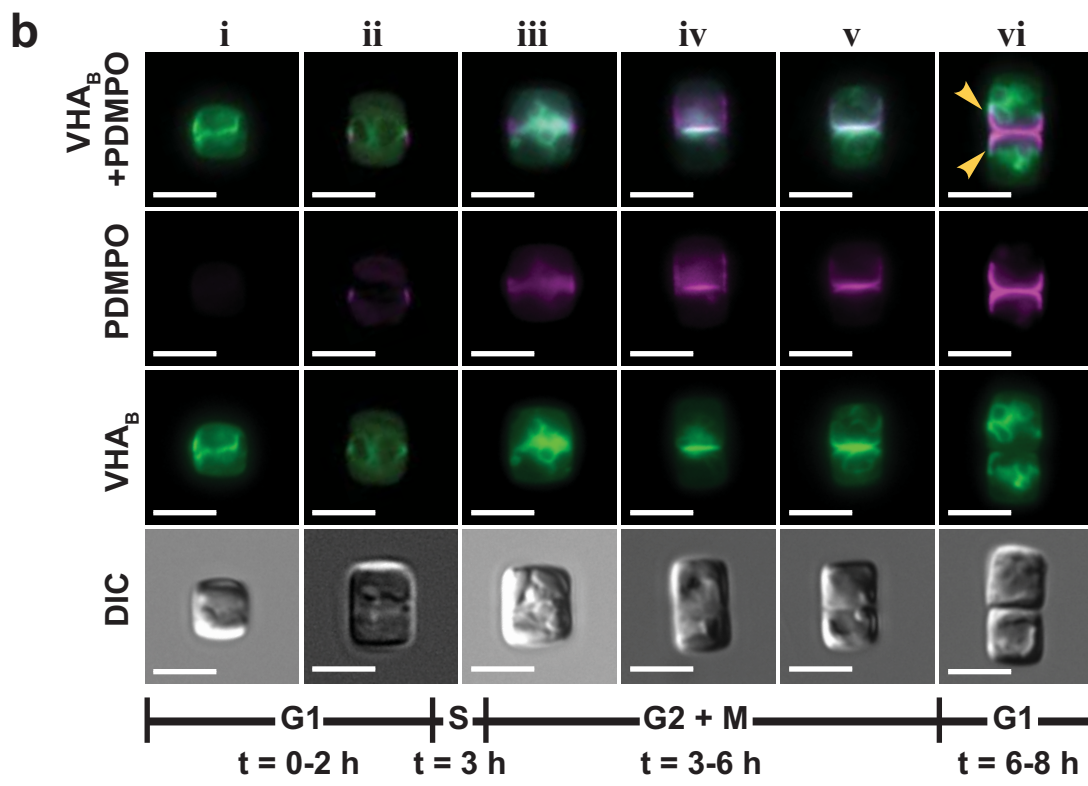
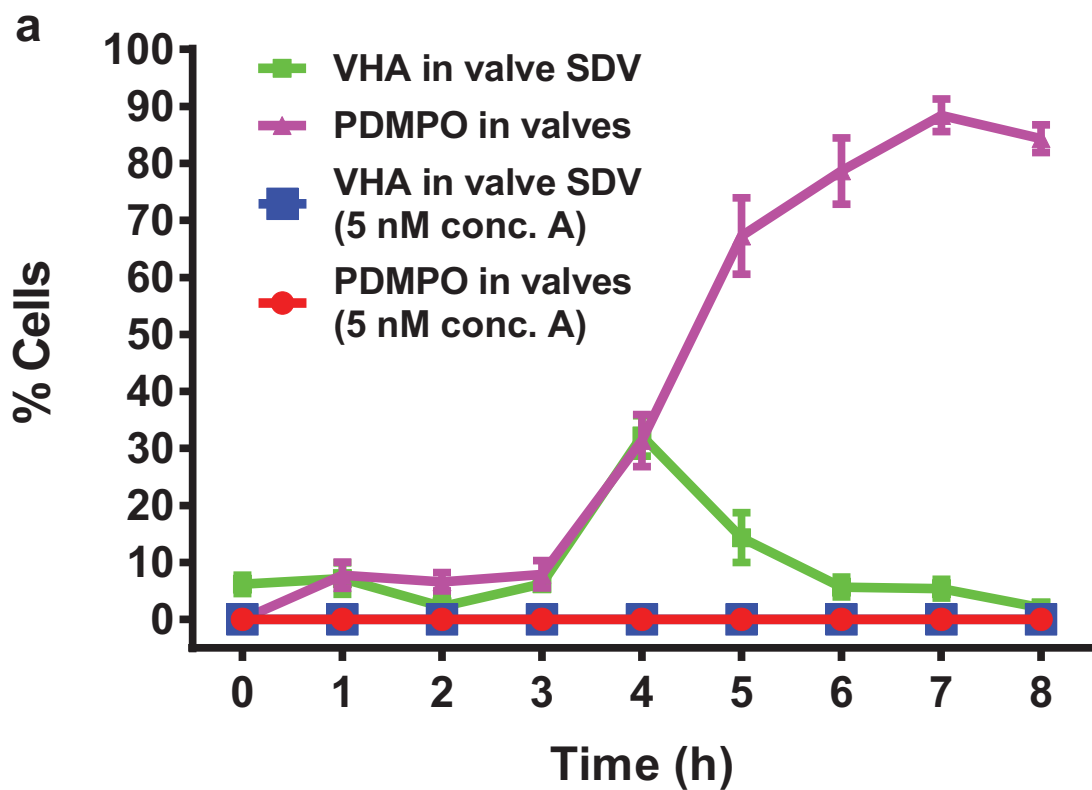
**Video S2** Time-lapse imaging video of *T. pseudonana* expressing fcp-VHA<sub>B</sub>-eGFP during girdle band biosynthesis [MP4 888 kb].







● native VHA-B    ■ VHA-B-eGFP    ▲ VHA-B mRNA



# 5 nM Concanamycin A

